Bioorganic Chemistry 82 (2019) 74–85

Contents lists available at ScienceDirect

Bioorganic Chemistry

journal homepage: www.elsevier.com/locate/bioorg

Pentamethinium salts as ligands for cancer: Sulfated polysaccharide co-receptors as possible therapeutic target

Tomáš Bříza [a,b,*], Jarmila Králová [c], Silvie Rimpelová [a], Martin Havlík [a,b], Robert Kaplánek [a,b], Zdeněk Kejík [b], Pavel Martásek [b], Ivan Mikula [b], Petr Džubák [d], Marián Hajdúch [d], Tomáš Ruml [a], Vladimír Král [a,b,*]

[a] University of Chemistry and Technology, Prague, Technická 5, 166 28, Prague 6, Czech Republic
[b] First Faculty of Medicine, Charles University in Prague, Kateřinská 32, 121 08, Prague 2, Czech Republic
[c] Institute of Molecular Genetics, Academy of Sciences of the Czech Republic, Vídeňská 1083, 142 20, Prague 4, Czech Republic
[d] Institute of Molecular and Translational Medicine, Hněvotínská 5, 779 00 Olomouc, Czech Republic

ARTICLE INFO

Article history:
Received 7 September 2017
Revised 2 February 2018
Accepted 10 February 2018
Available online 16 February 2018

Keywords:
Anticancer activity
Cytotoxicity
Fluorescent cyanine
Pentamethinium salt
Recognition
Sulfated polysaccharides

ABSTRACT

A series of pentamethinium salts with benzothiazolium and indolium side units comprising one or two positive charges were designed and synthesized to determine the relationships among the molecular structure, charge density, affinity to sulfated polysaccharides, and biological activity. Firstly, it was found that the affinity of the pentamethinium salts to sulfated polysaccharides correlated with their biological activity. Secondly, the side heteroaromates displayed a strong effect on the cytotoxicity and selectivity towards cancer cells. Finally, doubly charged pentamethinium salts possessing benzothiazolium side units exhibited remarkably high efficacy against a taxol-resistant cancer cell line.

1. Introduction

Cell-cell communication is essential for multicellular organisms. Every cellular process, including cell growth, death, and differentiation, depends on the activity and pathways of signaling molecules. Aberrant changes in the system of cell-to-cell communication may result in various pathological states, such as cancer, chronic inflammatory disorders, and autoimmune diseases [1]. The involved pathological signaling pathways seem to represent attractive targets for a therapeutic intervention.

A common way to modulate, inhibit or activate cell-to-cell communication is based on exploitation of specific chemical ligands targeting individual components of the signaling pathways, such as signaling molecules and their corresponding receptors. However, the therapeutic strategy affecting only one target has not proved to be very effective and often resulted in resistance. At present, a new concept involving molecules interfering simultaneously with multiple targets is being explored as a more efficient strategy [2–4]. Such an approach might enable low-dose administration of active agents resulting in elimination of possible undesired adverse effects and producing additional synergistic or additive therapeutic results. The design of multi-targeted chemical ligands should be based on a chemical structure of their respective

Abbreviations: A549, cells of lung adenocarcinoma; AIDS, acquired immune deficiency syndrome; BJ, human fibroblasts (non-malignant cell line); BrdU, 5-bromo-20-deoxyuridine; BrU, 5′-bromouridine; CEM, cells of *T*-lymphoblastic leukemia; CEM-DNR-bulk, cells of *T*-lymphoblastic leukemia overexpressing Multidrug resistant protein 1; CHO-K1, Chinese hamster ovary; DMEM, Dulbecco's Modified Eagle Medium; DMF, dimethylformamide; DMSO, dimethylsulfoxide; FITC, fluorescein-isothiocyanate; GAG, glycosaminoglycans; HCT116, cells of colorectal cancer with wild type p53; HCT116p53−/−, colorectal cancer cell line with deleted p53; IC_{50}, drug concentration lethal for 50% of cells; K562, myeloid leukemia cell line; K562-TAX, myeloid leukemia cells overexpressing P-glycoprotein; Ks, Conditional constant; LNCaP, prostatic carcinoma cells; MCF-7, breast cancer cell line; MiaPaCa-2, cells of pancreatic carcinoma; MRC-5, human fibroblasts (non-malignant cell line); MTT, thiazolyl blue tetrazolium bromide; NF-κB, nuclear factor kappa-light-chain-enhancer of activated B cells; OD, optical density; PAGE, polyacrylamide gel electrophoresis; PBS, phosphate buffered saline; PEI, polyethylenimine; RPMI 1640, Roswell Park Memorial Institute 1640 medium; SD, standard deviation; SDS, sodium dodecyl sulfate; SI, selectivity index; TNF-α, tumor necrosis factor alpha; U-2 OS, osteosarcoma cell line.

* Corresponding authors at: Department of Pediatrics and Adolescent Medicine, First Faculty of Medicine, Charles University in Prague, Kateřinská 32, 121 08, Prague 2, Czech Republic.

E-mail addresses: tomas.briza@vscht.cz (T. Bříza), vladimir.kral@vscht.cz (V. Král).

https://doi.org/10.1016/j.bioorg.2018.02.011
0045-2068/

targets. Therefore, the structure of growth factor receptors commonly overexpressed on the surface of cancer cells should be the main clue for the design of rational synthetic ligands. However, due to a very complex nature of these protein receptors, it is very difficult to achieve their identification by specific recognition and targeting. Importantly, several reports indicated that the saccharide parts of the growth factor receptors, sulfated glycosaminoglycans (GAG), are essential for the receptor function on cancer cells. This fact was favorably exploited for their detection and recognition [5–7] and directed our design of multitargeted ligands by focusing on polysulfated GAGs.

Polysulfated GAGs (e.g. heparan sulfate, chondroitin sulfate) are polysaccharides with high structural variability, possessing a negative charge due to sulfate and carboxyl groups. The average number of GAG modifications is one sulfate and one carboxyl group per one repeating disaccharide unit. The GAGs are functional, long unbranched heteropolysaccharides playing a key role in regulation of a number of cellular events as well as physiological and pathological processes [8]. Their biological function generally depends on the interactions of the binding domain (highly sulfated part of GAGs) with signal factors (cytokines and soluble growth factors) [9]. Changes in GAGs overexpression undoubtedly influence proliferation of cancer cells, metastasis, and tumor progression [10,11] Therefore, targeted inhibition of the expression [12] or glycosylation [13] of these co-receptors can lead to reduction of the tumorigenic phenotype, metastatic potential and angiogenesis. Polysulfated GAGs also play a role in other serious pathophysiological settings, including amyloid diseases (Alzheimer's disease; serum amyloid A protein, transthyretin-related amyloidosis and amyloid light-chain amyloidosis, type 2 diabetes, Parkinson's disease, amyotrophic lateral sclerosis and prion diseases) [14], infectious diseases (severe anemia, respiratory distress, cerebral ischemia and AIDS) [15–18], inflammatory conditions and some developmental disorders [19,20]. In the amyloid genesis, sulfated GAGs bind amyloid proteins and contribute to their aggregation in a fibrillar insoluble form [21]. They also protect the formed aggregates against proteolysis and probably facilitate stimulation of nitric oxide production and tumor necrosis factor alpha (TNF-α) expression [22,23]. Even though the amyloid proteins are structurally unrelated, they share the ability to bind sulfated GAGs, which could be envisaged as a potential therapeutic target in amyloid genesis. Several groups reported positive correlation of the sulfation degree of the used polysaccharides with the change of their conformation states [24–26] thereby indicating the importance of the sulfated part of GAGs. In agreement with this hypothesis, a higher level of sulfated GAGs was observed in human brains (post-mortem) affected by amyloid diseases [22,27].

On the other hand, sulfated GAGs can serve as therapeutic agents for treatment of cancer, viral and bacterial infections, or blood clotting [28–30]. All these facts indicate a high clinical potential of sulfated GAGs, which could be specifically recognized and targeted through their highly sulfated domains. To our best knowledge, the detection of sulfated polysaccharide receptors is an unexplored area. In theory, a suitable tool for recognition of anionic polymers, such as GAGs, might be cationic ligands. Furthermore, the structural motif for GAG-specific ligands should also include, beside the cationic charge motif (binding the anionic sulfate group), heteroaromatic groups (binding the saccharide part) [31]. Interestingly, our team also achieved recognition of heparan sulfate by generating bile acid porphyrin conjugates [6]. The inspiration for this approach arose from already reported sensors recognizing an extensively sulfated polysaccharide, heparin [32–34].

Previously, we reported a significant spectral response of the pentamethinium structural motif in the presence of sulfated polysaccharides (namely heparin) [35]. However, the hydrophobicity of pentamethinium salts and their strong aggregation in aqueous solutions required admixture of organic solvents negatively influencing the desired interactions. Therefore, in this work we aimed to develop chemical ligands based on the pentamethinium system with high selectivity towards the sulfated polysaccharides in aqueous media at pH 7.34 allowing applicability at physiological conditions. Our goal was to confirm the hypothesis that the affinity of chemical ligands consisting of pentamethinium salts correlates with the amount of anionic sulfate groups in the studied analytes resembling cancer receptors. The issue of the pentamethinium system hydrophobicity [35,36] required redesign of the structure to ensure sufficient hydrophilicity, and, additionally, charge variability of the whole system. The most frequently used method for enhancing hydrophilicity of largely hydrophobic compounds is substitution with alkyl sulfate groups [37–39], but this approach was not feasible due to possible interferences with the tested analytes. Our strategy to achieve higher hydrophilicity and to increase charge density of the pentamethinium system was based on the introduction of a second positive charge by nitrogen quarternization. Some of γ-substituted pentamethinium salts described in our previous work contained a pyridyl substituent in the *meso*-position [40], the presence of which offers the possibility of nitrogen quarternization, and therefore these salts were included in the presented study.

2. Results and discussion

The aim of this work was to study and compare monocationic and corresponding dicationic pentamethinium salts, and to elucidate the influence of the second positive charge and a side heteroaromatic unit (benzothiazolium or dimethylindolium) on their biological properties. Our strategy was based on the selection of structures that could be quarternized to the second stage by a methyl group. The most feasible way to do this is utilization of pentamethinium salts substituted in γ-position by a pyridyl unit, which can be further quarternized. Preliminary biological tests were performed to find out whether a substituent other than pyridyl in the γ-position or a different substituent on a heterocycle shows a difference in cancer cell selectivity.

As a starting point for design and synthesis, two positively charged pentamethinium derivatives, **1** and **3**, were selected as suitable ones for quarternization. The quarternization step has been already described for derivative **1** with benzothiazolium units in our previous study [40]. In summary, four compounds, **1**–**4**, differing in the number of positive charges and possessing either benzothiazolium or indolium side units, were included in this study.

First, we assayed the affinity of compounds **1**–**4** to the selected sulfated polysaccharides in aqueous medium. When positive results were obtained, we performed tests on cancer cell lines to assess the potential relationship between the affinity of the compounds to sulfated polysaccharides and their biological activity.

Pentamethinium salts **1** and **3** were alkylated with methyl to produce salts **2** and **4**, respectively (Scheme 1). Salt **1** was excluded from further studies due to insufficient solubility in aqueous medium, whereas salt **3** was included as sufficiently soluble under the selected conditions. As expected, doubly positively charged salts **2** and **4** exhibited significantly increased solubility in aqueous medium than mono-positively charged salts **1** and **3,** respectively.

2.1. Study of pentamethinium salt affinity to sulfated polysaccharides

The affinity of potential chemical ligands **2**–**4** to sulfated polysaccharides was assayed by UV–Vis spectroscopy. In this assay we followed the impact of the negative charge and a sulfation degree of a disaccharide unit on the interactions with sulfated polysaccharides. The selected analytes included β-glucan, hyaluro-

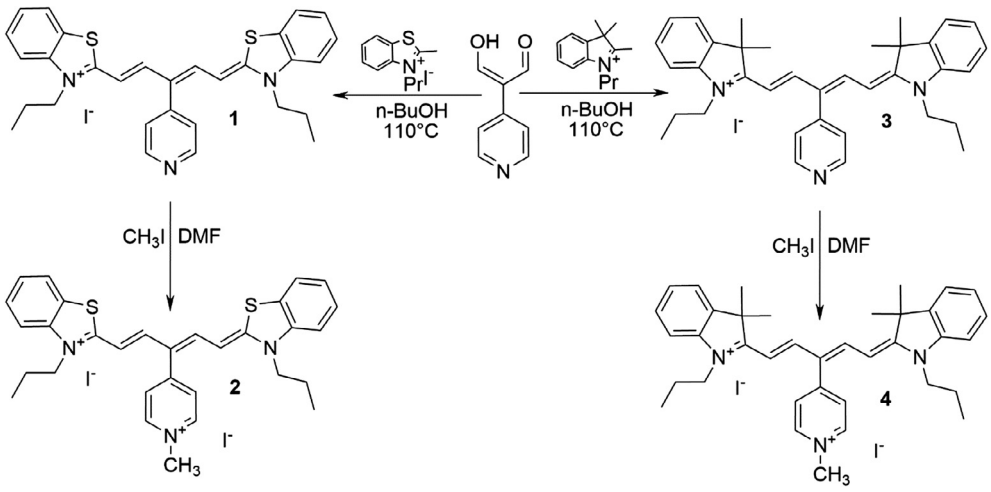

Scheme 1. Synthesis of salts **1**–**4** based on a pentamethinium system.

nic acid and alginic acid completely lacking sulfate groups (serving as controls), heparin with three sulfate units, and dextran sulfate with the highest density of sulfate groups per one disaccharide unit (Table 1). The binding constants of salt **2** with the tested analytes were found moderately augmented with the increasing number of negative charges per a disaccharide unit (Table 1).

In comparison, the salts **3** and **4** displayed lower affinity for targeted sulfated polysaccharides, albeit with a similar preference for polysaccharides with a higher number of anionic groups as salt **2**. The affinity of salt **3** for the tested analytes was dependent on the presence of sulfated groups (comparing analytes with the same overall charge density), depicted in Table 1. Salt **3** showed affinity for sulfated polysaccharides, chondroitin sulfate and heparan sulfate with Log(K) equal to 4.7 and 4.3, respectively. Log(K) for non-sulfated polysaccharide, alginic acid, was equal to 3.5. Salt **4** with two positive charges did not show this preference. We did not observe any significant interaction of tested salts **2**–**4** either with hyaluronic acid or with β-glucan. The obtained data showed that the affinity of the tested salts for anionic polysaccharides was dependent on the number of their anionic, especially sulfate groups.

On the other hand, when we increased the hydrophobicity of the salt environment by adding methanol (H_2O:MeOH; 2:1), this led to a significant reduction in their affinity for heparin. This fact indicates that the affinity of the tested polymethinium salts for anionic polysaccharides can be influenced by other phenomena than solely by electrostatic interactions. In according with this, the most hydrophobic salt **4** displayed a different interaction mode than that of **2** and **3**. Its high hydrophilicity suppressed its aggregation in the presence of anionic polysaccharides; one polysaccharide unit did not interact with more molecules of salt **4**. On the other hand, due to the fact that this poorly aggregated salt **4** carries two positive charges, it can interact with two polysaccharide units. Salt **2** carries also two cationic charges but it is significantly more hydrophobic than salt **4**. Aggregation of thiacarbocyanine dyes in the presence of carboxylate and sulfate polymers was described also in other studies (35,46). Due to the abovementioned and the charge density of the tested anionic polysaccharides, possible binding modes include interaction of a polysaccharide unit with one or more molecules of salt **2**. Salt **3** is not as hydrophobic as salt **2** but, since it carries only one cationic charge, it is significantly less hydrophilic than salt **4**. Which implies that salt **3** can interact with only one polysaccharide unit of the tested analytes but one polysaccharide unit can bind more molecules of salt **3**. All results regarding the binding constants of salts **2**–**4** with sulfated polysaccharides are summarized in Table 1.

Table 1
The influence of charge density and sulfation degree on the affinity of salts **2–4** to polysaccharides in aqueous medium (H_2O:MeOH; 99:1).

Polysaccharide	Charge density[a]	Sulfate groups[b]	Log(K)/M and complex stoichiometry[c]		
			Salt 2	Salt 3	Salt 4
β-Glucan	0	0	n.d.[d]	n.d.	n.d.
Hyaluronic acid	−1	0	n.d.	n.d.	n.d.
Alginic acid	−2	0	4.80 (1:1)	3.50 (1:1)	5.80 (1:1) 8.30 (2:1)
Chondroitin sulfate	−2	1	5.60 (1:1) 12.0 (1:2)	4.76 (1:1) 10.7 (1:2)	5.50 (1:1) 7.20 (2:1)
Heparan sulfate	−2	1	5.80 (1:1) 12.3 (1:2)	4.30 (1:1) 10.7 (1:2)	4.10 (1:1) 8.90 (2:1)
Heparin	−4	3	11.2 (1:2) 17.3 (1:3)	10.8 (1:2)	5.17 (1:1) 10.4 (2:1)
Heparin (H_2O:MeOH; 2:1 (v/v))			4.70 (1:1) 9.70 (1:2)	n.d.	n.d.
Dextran sulfate	−4	4	34.0 (1:4)	10.7 (1:2)	4.80 (1:1) 11.0 (2:1)

[a] Electrical charge per polymer unit – number of anionic groups (carboxylate, sulfate) per disaccharide unit [41–45].
[b] Number of sulfate groups per disaccharide unit [41–45].
[c] Ratio of analyte vs. tested salt.
[d] not determined.

UV–Vis analysis showed that the interaction of the selected sulfated polysaccharides (chondroitin sulfate and heparan sulfate) with salt **2** led to partially decreased intensity of the original absorbance band and to emergence of a new spectral band around 530 nm (blue shift) (Fig. 3). Salts **3** and **4** displayed only decreased intensity of the original band without appearance of a new band as in the case of salt **2**. The intensity of this newly emerged band at 530 nm increased with the number of sulfate groups per a disaccharide unit. In case of hyaluronic and alginic acids (Fig. 1A and B), no new bands were observed in this region, which was probably caused by the absence of sulfate groups. This phenomenon could be caused by aggregation of salt **2** in the presence of sulfate saccharides. It has been reported previously that methinium salts of a benzothiazolium type form H-aggregates with a typical blue shift in the presence of anionic carboxylic and sulfated polymers [46,47].

To better understand the role of aggregation in the interaction of salt **2** with sulfated polysaccharides, we performed a titration study of compound **2** with heparin in medium with a larger portion of organic solvent (H_2O:MeOH; 2:1), see Fig. 2B. It is well known that some organic solvents, such as methanol, can inhibit aggregation of polymethinium salts [40]. A slight suppression of the blue shift was observed in the area of 530 nm (Fig. 2), as expected. Besides that, the values of calculated interaction constants were decreased (Table 1).

The observed blue shift was probably caused by self-assembly (H-aggregates) of salt **2** on the surface of sulfated polysaccharides in aqueous surroundings. Chondroitin and heparan sulfates, representing analytes with one sulfate group per a disaccharide unit, exhibited a weaker response to salt **2** in this area of the spectra (Fig. 3) compared to heparin.

Dextran sulfate, an analyte with four sulfate groups, displayed the strongest blue shift with a new maximum at 530 nm, likely due to the highest density of anionic charges and the highest number of sulfate groups per one disaccharide unit (Fig. 4).

The intensity of the response to sulfated polysaccharides was affected not only by the increasing density of anionic charge but also by the number of sulfate groups. We assume that the interaction of sulfated polysaccharides with the salts was accompanied by formation of H-aggregates, as manifested by the titration studies with salt **2** (Figs. 2–4). The formation of H-aggregates most likely does not depend on the number of carboxyl groups, but at least one sulfate group on the polysaccharide surface seems to be substantial. It has been demonstrated experimentally that in the presence of hyaluronic acid (one carboxyl group) and alginic acid (two carboxyl groups), no formation of H-aggregates, causing the blue shift, occurred (Fig. 1). A clear correlation between the numbers of sulfate groups and the intensity of response in the blue area was demonstrated for an interaction of salt **2** with heparin (three sulfate groups) and dextran (four sulfate groups), Figs. 2 and 4, respectively.

To summarize our observations, high numbers of sulfate groups together with increased density of anionic charge of sulfated polysaccharides support the interaction of the analyte with the selected pentamethinium salts.

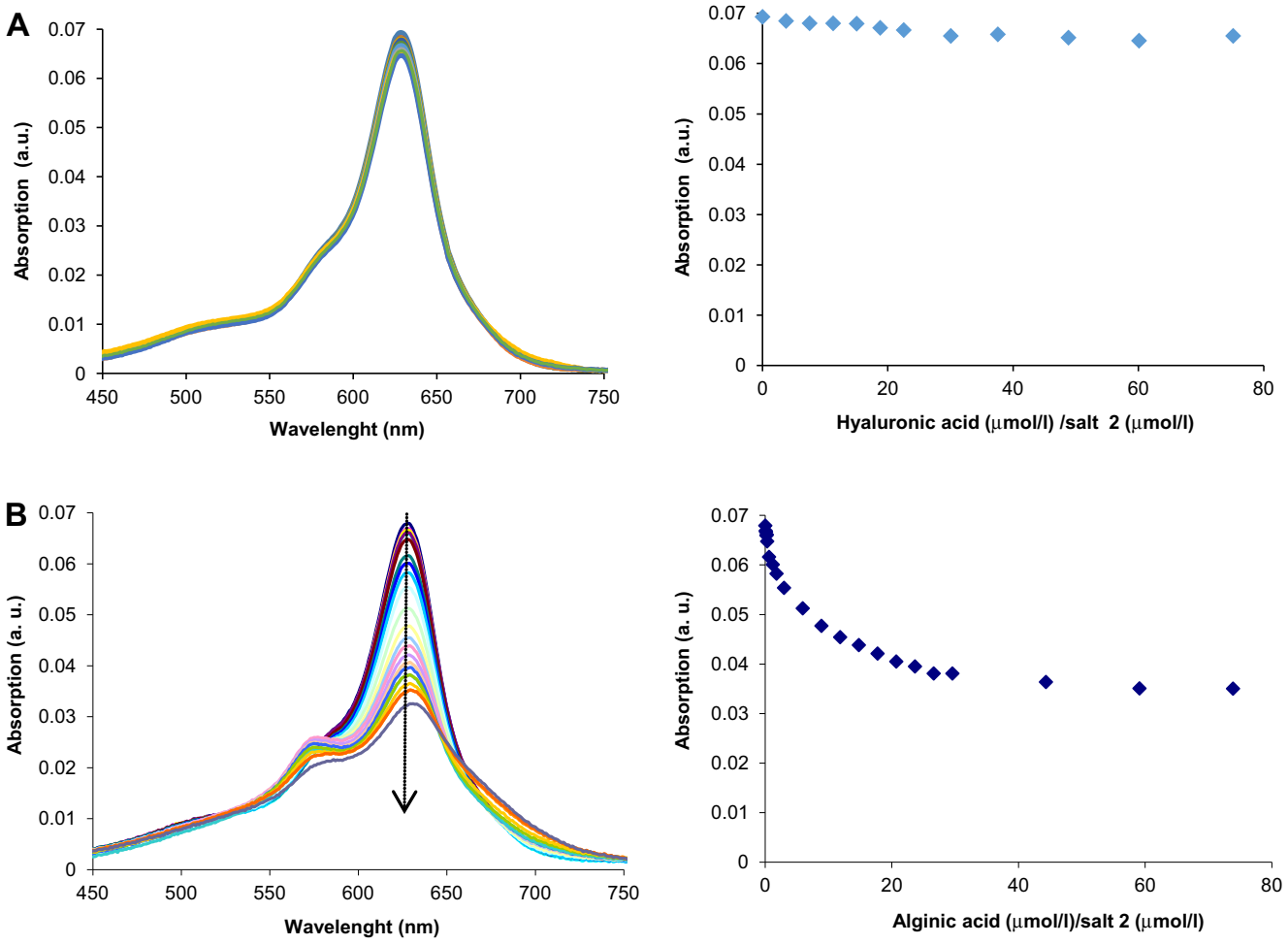

Fig. 1. UV–Vis titration and titration curves of salt **2** (1.8 μmol L^{-1}) in 1 mM phosphate buffer (H_2O:MeOH; 99:1 (v/v), pH 7.34) with (A) hyaluronic acid; (B) alginic acid.

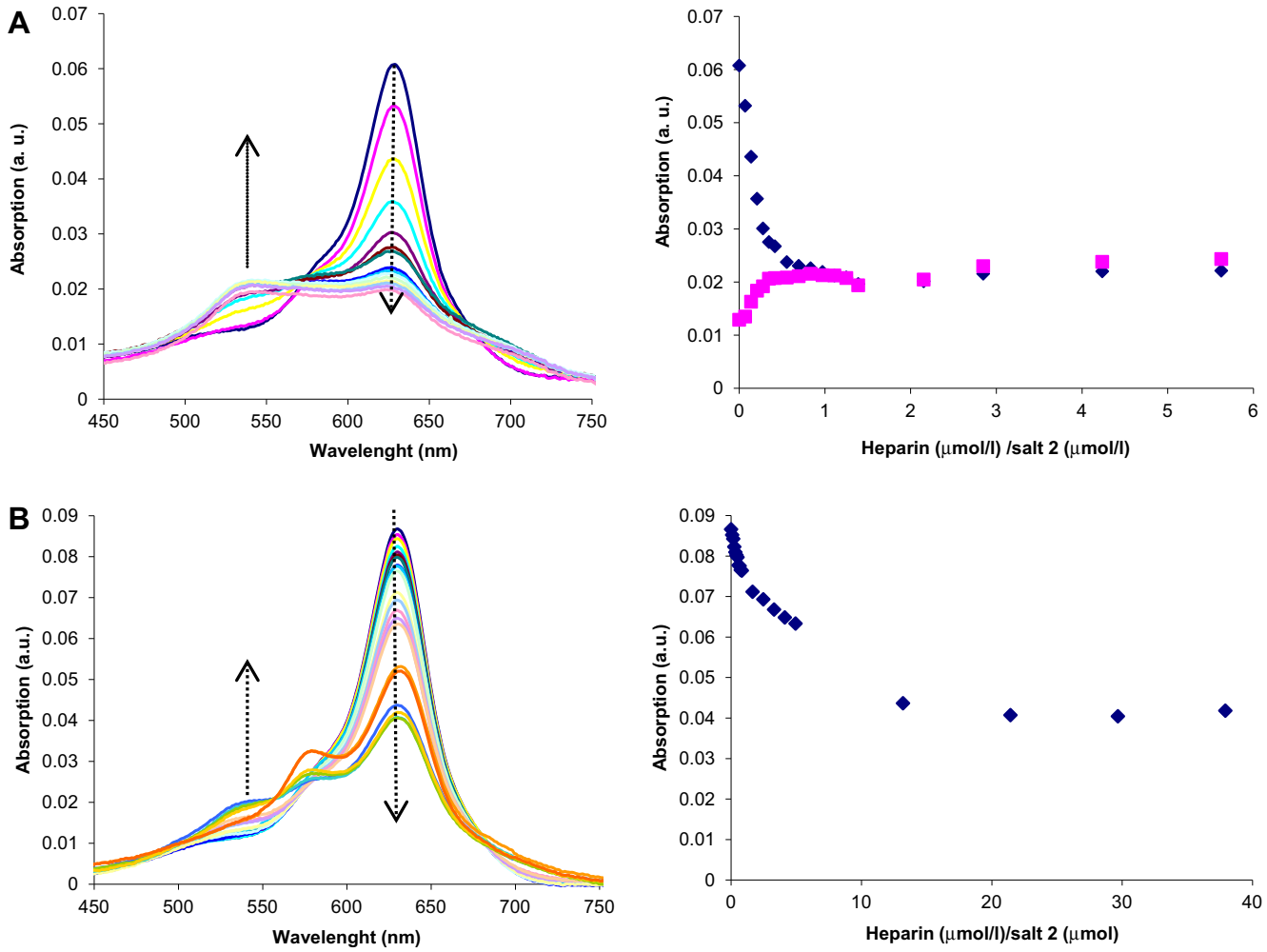

Fig. 2. UV–Vis titration and titration curves of salt **2** (1.8 μmol L^{-1}) with heparin in 1 mM phosphate buffer, pH 7.34. (A) H_2O:MeOH; 99:1 (v/v); (B) H_2O:MeOH, 2:1 (v/v).

2.2. In vitro cytotoxicity study

To make our study more comprehensive, we aimed to find the relationship between the chemical structures of the prepared compounds and their biological activity. The obtained results should reveal how their biological activity correlates with the affinity to the sulfated polysaccharides.

The cytotoxicity effects of the prepared polymethinium salts **1**–**4** were tested *in vitro* by MTT assay using 11 human cancer cell lines: CEM (T-lymphoblastic leukemia), K562 (myeloid leukemia), their drug-resistant counterparts CEM-DNR-bulk (overexpressing Multidrug resistant protein 1) and K562-TAX (overexpressing P-glycoprotein); A549 (lung adenocarcinoma), HCT116 (colorectal cancer with wild type p53), HCT116p53−/− (colorectal cancer with deleted p53), U-2 OS (osteosarcoma), MiaPaCa-2 (pancreatic carcinoma), LNCaP (prostatic carcinoma), and MCF-7 (breast cancer). Two fibroblast cell lines derived from human foreskin and lung, BJ and MRC-5, respectively, were used as non-malignant controls. The MTT (thiazolyl blue tetrazolium bromide) assay is based on the conversion of MTT substrate into formazan crystals by mitochondrial activity of metabolically active cells, which is directly linked to the number of viable cells, thus reflecting the *in vitro* cytotoxicity of the tested compounds [48].

Surprisingly, we detected significant differences between the compounds possessing benzothiazolium (thiodicarbocyanines **1** and **2**) and indolium (dicarbocyanines **3** and **4**) side units. While salts **1** and **3** with one positive charge showed comparable cytotoxicity, salts **2** and **4** with doubly positive charges displayed significant differences (Table 2).

The thiodicarbocyanine salt **2** induced cytotoxicity one order of magnitude higher than salt **4** in all tested cancer cell lines. This effect can be ascribed to the type of side units introduced in the pentamethinium structure. The highest difference was observed for K562-TAX line: the IC_{50} of compound **2** was 0.06 μM, whereas IC_{50} of **4** was >75.00 μM. Thus, in these cells, salt **2** was approximately ten thousand times more toxic than salt **4** (Fig. 5).

Another notable feature of salt **2** appeared in its cytotoxic selectivity. The cytotoxic selectivity was defined as a ratio of average IC_{50} obtained in the experiment with non-malignant cell lines (MRC-5 and BJ cells) and IC_{50} of a given relevant cancer cell line, similarly to literature specification [49,50]. Salt **2** displayed one order of magnitude higher selectivity towards cancer cell lines than the tested salts **1**, **3**, and **4** (Table 3, Fig. 6). Such a strong influence of a side unit on the selectivity of the pentamethinium motif for cancer cells over non-malignant cells is outstanding and indicates that the structural motif of pentamethinium salts with two cationic charges is very promising for design of novel anticancer drugs with high cancer cell selectivity.

On the other hand, dicarbocyanine salt **4** with two positive charges displayed much lower cytotoxicity in most of the tested cell lines in comparison to rest of the tested salts **1**–**3** and no selectivity for malignant cells. Accordingly, analytical titration did not show any preferences for sulfate polysaccharides, see Table 1.

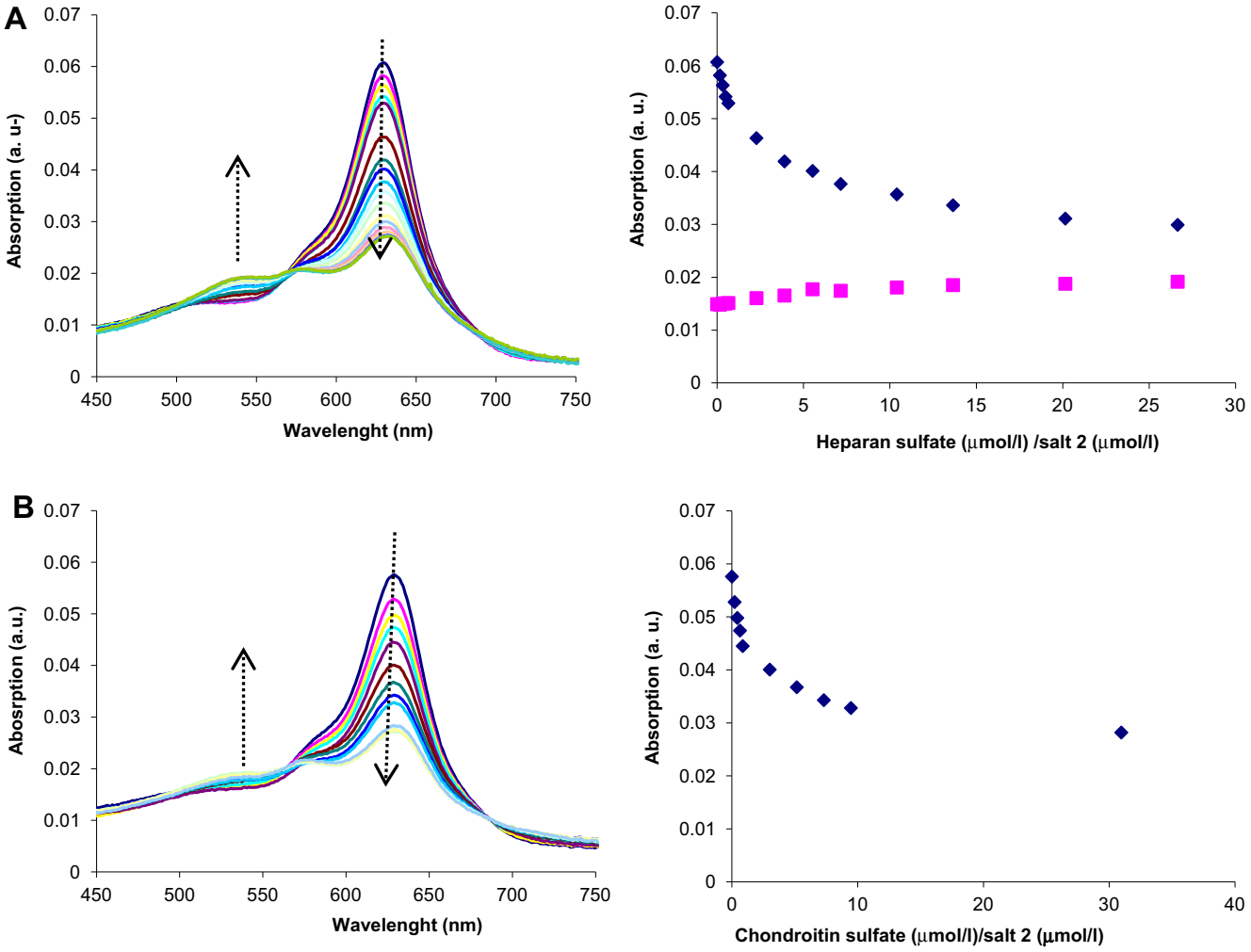

Fig. 3. UV–Vis titration and titration curves of salt **2** (1.8 μmol L^{-1}) with (A) chondroitin sulfate; (B) heparan sulfate in 1 mM phosphate buffer (H_2O:MeOH; 99:1 (v/v)), pH 7.34.

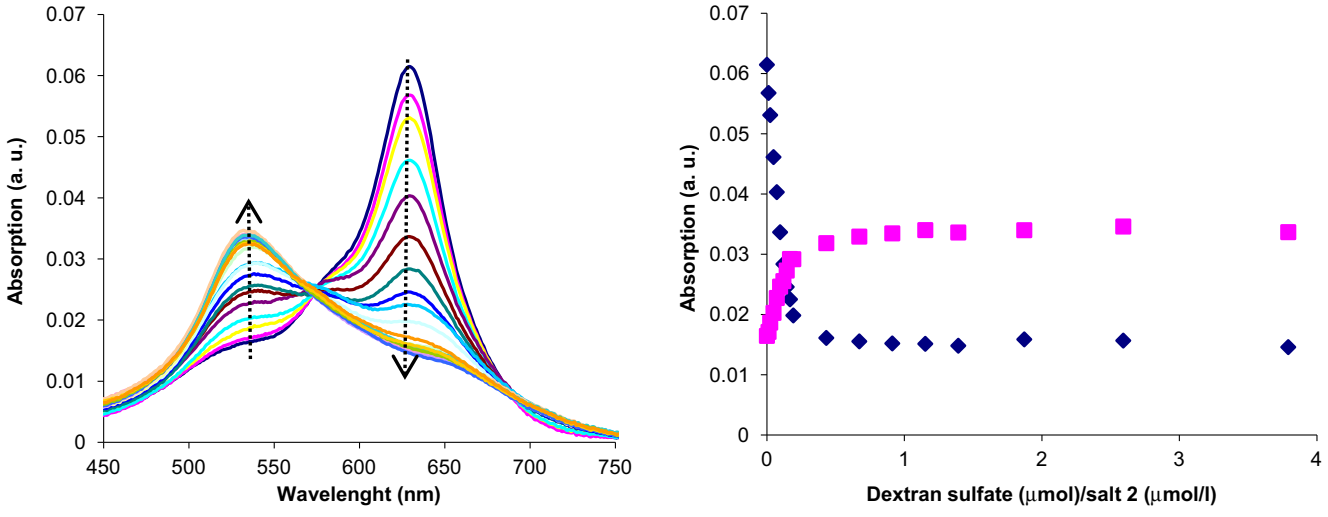

Fig. 4. UV–Vis titration and titration curves of salt **2** (1.8 μmol L^{-1}) with dextran sulfate in 1 mM phosphate buffer (H_2O:MeOH; 99:1 (v/v)), pH 7.34.

Interestingly, the cytotoxicity of salts **1** and **2** was approximately two times higher for a cell line with suppressed p53 protein activity, HCT116p53−/−, than for its original counterpart, HCT116. Similarly, Ferrandiz et al. observed decreased cytotoxicity of 5-fluorouracil, adriamycin, gefitinib and imatinib for a p53-deficient cell line when compared to the parental line, HCT116

Table 2
Cytotoxic activity of compounds **1–4** against cancer cell lines: A549, CCRF-CEM, CEM-DNR, HCT116, HCT116p53−/−, K562, K562-TAX, U-2 OS, MiaPaCa-2, LNCaP and MCF-7. BJ and MRC-5 cells are non-malignant cell lines (controls). The cells were incubated with the tested compounds for 72 h.

Cancer cell lines	IC_{50} [μM]			
	1	2	3	4
A549	0.26	0.25	0.11	72.10
CCRF-CEM	0.07	0.49	0.06	22.70
CEM-DNR	0.55	1.09	1.44	73.90
HCT116	0.22	0.93	0.10	66.40
HCT116p53−/−	0.50	1.71	0.12	69.90
K562	0.08	0.60	0.07	21.90
K562-TAX	0.05	0.06	0.37	>75.00
U-2 OS	4.90	19.01	1.05	>75.00
MiaPaCa-2	1.78	0.69	0.27	57.32
LNCaP	2.01	12.22	0.60	63.99
MCF-7	18.02	1.23	0.47	67.02
MRC-5	1.93	45.6	5.66	>75.00
BJ	2.04	55.0	3.28	>75.00

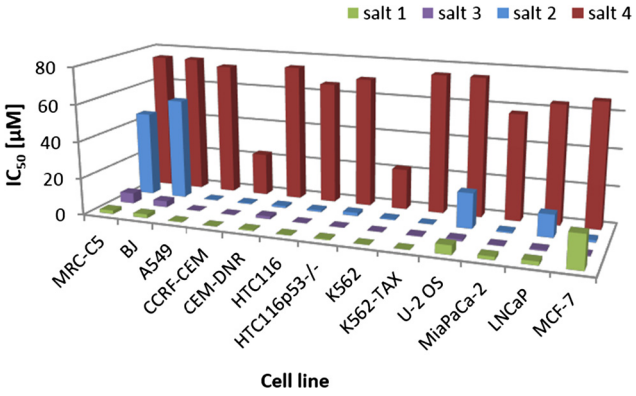

Fig. 5. Influence of the pentamethinium side units on *in vitro* cytotoxicity. Dependence of IC_{50} [μM] of compounds **1–4** on the tested cell lines. Cancer cell lines: A549, CCRF-CEM, CEM–DNR, HCT116, HCT116p53−/−, K562, K562-TAX, U-2 OS, MiaPaCa-2, LNCaP and MCF-7. BJ and MRC-5 cells served as controls representing non-malignant cell lines.

Table 3
Cytotoxic selectivity of compounds **1–4** for A549, CCRF-CEM, CEM–DNR, HCT116, HCT116p53−/−, K562, K562-TAX, U-2 OS, MiaPaCa-2, LNCaP and MCF-7 cell lines.

Cancer cell lines	Cytotoxic selectivity of salts 1–4			
	1	2	3	4
A549	7.63	201.20	40.64	1.04
CCRF-CEM	28.36	102.65	74.50	3.30
CEM-DNR	3.61	46.15	3.10	1.01
HCT116	9.02	54.09	44.70	1.13
HCT116p53−/−	4.00	29.42	37.25	1.07
K562	25.80	83.83	63.85	3.42
K562-TAX	36.80	838.33	12.08	1.00
U-2 OS	0.41	2.65	4.26	1.00
MiaPaCa-2	1.12	72.90	16.56	1.31
LNCaP	0.99	4.12	9.51	1.12
MCF-7	0.11	40.90	7.45	1.17

[51]. Moreover, although cytotoxicity of salt **3** was significantly higher than cytotoxicity of thiodicarbocyanine salts **1** and **2**, it did not show any difference between HCT116 cells and their corresponding counterparts without p53 expression.

These results indicate that the effect of salts **1** and **2** might be, at least partially, based on the activation of cell cycle arrest and apoptosis signaling pathways impacted by p53 protein, while the anti-

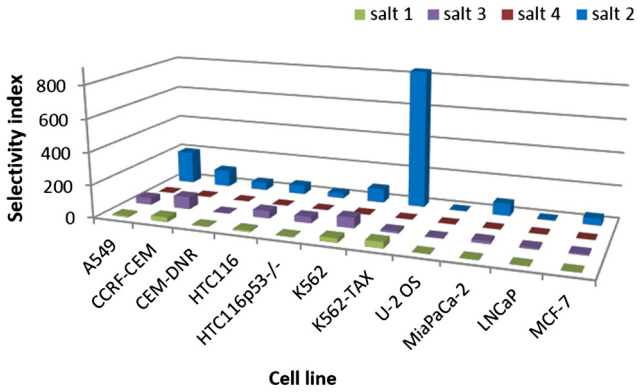

Fig. 6. Cytotoxic selectivity of salts **1–4** for A549, CCRF-CEM, CEM–DNR, HCT116, HCT116p53−/−, K562, K562-TAX, U-2 OS, MiaPaCa-2, LNCaP and MCF-7 cell lines.

cancer effects of carbocyanine salts **3** and **4** are probably not dependent on the above-mentioned factors.

Thiodicarbocyanine salts **1** and **2**, but mainly salt **2**, displayed higher cytotoxicity against a resistant cell line K562-TAX than against its parental cell line, whereas carbocyanine salts **3** and **4** manifested an opposite trend. It is well known that taxol resistance of leukemic cells K562 is coupled with a significantly higher expression level of NF-κB (nuclear factor kappa-light-chain-enhancer of activated B cells) [52]. Its higher expression level can positively influence the activity of growth factors and interleukin signaling pathways [53]. IC_{50} values of thiodicarbocyanines indicate that this structural motif can target signaling pathways coupled with the above-mentioned phenomena.

The potential impact of the tested compounds on NF-κB signaling was assayed using NF-κB luciferase reporter. HCT116 cells were transiently transfected with reporter plasmids for 24 h and subsequently treated with salts **2** and **4** for indicated times before analysis. The NF-κB reporter activity in cell lysates was significantly stimulated by salt **2**, but only marginally by salt **4** (Fig. 7A). Cells transfected with a control plasmid without NF-κB binding sites did not display any increase in luciferase activity above the background level following treatment with the salts (data not shown). These results clearly demonstrate that the activation of luciferase reporter by salt **2** is dependent on the presence of NF-κB binding sites. The activation of NF-κB was further confirmed by Western blot analysis showing a phosphorylation peak of NF-κB p65 at 6 h time point (Fig. 7B, top panel). The total expression of NF-κB p65 was elevated by the salt treatment during the time interval 6–24 h (Fig. 7B, middle panel). These results clearly demonstrate selective activation of NF-κB signaling in HCT116 cells by salt **2** and suggest the involvement of this pathway in cell death induced in other tumor cell lines as well. Although NF-κB is mainly known as a transcription factor protecting apoptosis, more recent reports illustrate a deeper complexity to the paradigm in which p53 drives cell death and NF-κB promotes cell survival. It is becoming clear that under some circumstances p53 can promote cell survival, while NF-κB can participate in the activation of cell death [54,55]. The striking difference in the cytotoxic effect of salt **2** towards transformed cells (tumor cell lines) and normal (non-transformed) cells likely relates to the abundance of sulfated polysaccharides on the surface of cancer cells, to which we have shown binding selectivity *in vitro*. However, the exact association between selective binding and the mechanism of NF-κB activation, whether direct or indirect, still remains to be elucidated.

A further objective of our study was to prove that removal of GAG chains from the cell surfaces affects the pentamethinium salt activity. To prove this hypothesis, we selected two models.

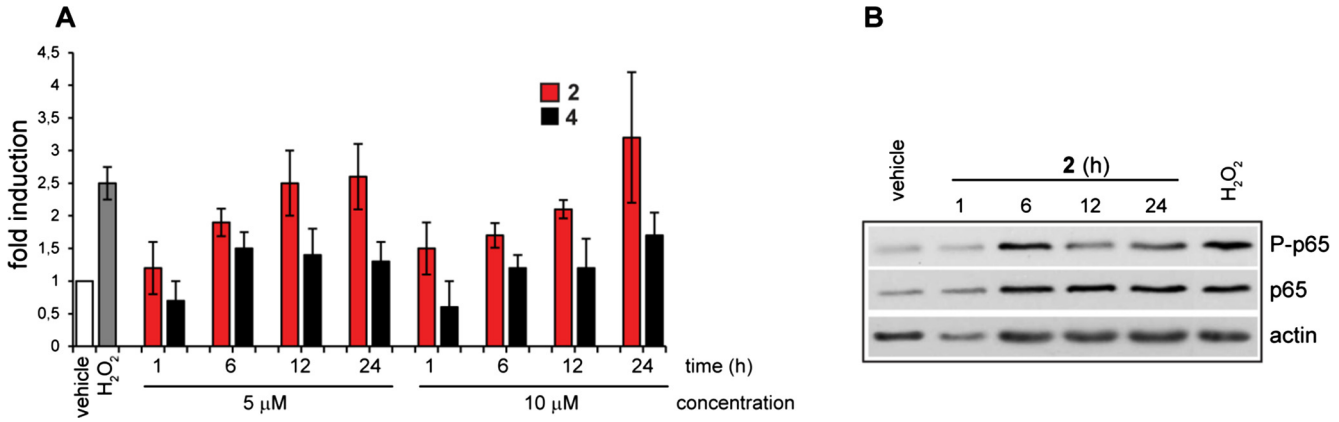

Fig. 7. Activation of NF-κB by salt **2**. (A) Activation of NF-κB luciferase reporter in HCT116 cells. Cells transfected with reporter plasmids were incubated one day after transfection in the presence of compound **2** (10 μM) or vehicle (DMSO) for the indicated times as described in . As positive control we used cells treated with H_2O_2 (500 μM) for 2 h. (B) Phosphorylation of NF-κB demonstrated by Western blot. Cell extracts were prepared, fractionated by 10% SDS-PAGE electrophoresis, electrotransferred to nitrocellulose membrane and subjected to Western blot analysis using Phospho-NF-κB p65 (Ser536) antibody and NF-κB p65 antibody. Anti-β-actin antibody was used to control sample loading.

First, we attempted to remove surface GAGs from human lung carcinoma cells (A549) by a chemical method using sodium chlorate, as reported by Schowalter, et al. [56]. As a control we employed non-treated A549 cells. The concentration of sodium chlorate was adjusted for the cells to survive but to remove the largest possible amount of GAGs. Cells were incubated with or without 25, 35 and 50 mM sodium chlorate for at least two weeks and then exposed to various concentrations of salts **1**–**4** (50–500 nM) for times ranging from 10 min up to 24 h, and monitored by live-cell fluorescence microscopy. Compounds **1**–**3** were localized in mitochondria already within 10 min. In contrast, compound **4** was extensively bound in extracellular parts of the cells. This observation fully substantiates the high IC_{50} values for salt **4**, which only marginally crossed the plasma cell membrane (Table 2). The localization kinetics for salts **1**–**3** was monitored immediately after adding the individual compounds and recorded for 12.5 min. However, we did not observe any difference either in the kinetics of intracellular localization of salts **1** and **3** (the localization course for the most selective salt **2** was not possible to record due to its insufficient photostability), or in the cytotoxicity of the salts **1**–**4** between treated and non-treated cells (data not shown). A possible explanation might be insufficient removal of GAGs from cell surfaces using sodium chlorate.

As a second model we used the pgsA-745 cell line, which is a Chinese hamster ovary (CHO-K1) cell mutant deficient in xylosyltransferase (UDP-d-xylose:serine-1,3-d-xylosyltransferase). Cells having this defect in xylosyltransferase, the first sugar transfer in glycosaminoglycan synthesis, do not produce GAGs. As a positive control, we used their parental cell line, CHO-K1. The live-cell fluorescence microscopy was performed after adding salts **1**–**4** to both cell lines, similarly as described above for control A549 cells. In both cases parental and mutant cells were able to transport salts across the membrane, indicating that the internalization mechanism was not disrupted. Importantly, primary recognition effect was identified in short time as a slightly delayed kinetics of intracellular localization of salts **3** and **1** in pgsA-745 cells in comparison to that in parental CHO-K1 cells. For example, compound **3** was intracellularly detectable already within 105–120 s after adding to CHO-K1 cells, but only after 165 s in pgsA-745 cells (see Supplementary video 1 and 2, Supplementary Fig. S13). This observation supports our hypothesis that the presence of GAGs on the cell surface plays an important role in the recognition of pentamethinium salts, and thus it might even facilitate their cellular entry. However, when the impact of GAGs presence on the salt toxicity was examined, despite of the difference in the uptake kinetics, these were not significantly reflected in the IC_{50} values after 72 h of incubation with the tested compounds. The IC_{50} profiles were comparable for both cell lines (Supplementary Fig. S14).

In summary, our experiments demonstrated that pentamethinium salts localize inside eukaryotic cells very quickly, thus the difference in localization kinetics in cells with and without GAGs on the cell surface might be erased after prolonged incubation period. Taking the uptake fast kinetics into consideration, current methods available to distinguish the role of specific ligand recognition from its causal impact are very limited. Moreover, in GAGs negative cells other compensatory mechanisms, avoiding

Table 4
Summary of cell cycle and DNA/RNA analysis of CCRF-CEM cells treated with the most potent compounds **1**–**3**. Data are expressed as a percentage of positive cells in the total cell population.

Compound	IC_{50}	Conc. (μM)	Sub G1[a] (%)	G0/G1 (%)	S (%)	G2/M (%)	pH3 Ser10 (%)	DNA synth. (%)	RNA synth. (%)
Control		0.00	3.58	36.52	37.46	26.03	1.10	43.84	32.98
1	1x[b]	0.07	2.61	35.74	34.02	30.24	1.16	44.69	41.23
	5x[c]	0.36	3.55	43.09	28.24	28.67	0.87	20.49	78.09
2	1x	0.49	6.24	38.50	38.10	23.40	1.01	44.47	27.74
	5x	2.43	60.70	43.33	30.32	26.35	0.85	35.98	55.42
3	1x	0.06	3.29	44.95	28.84	26.21	0.98	36.10	33.84
	5x	0.29	9.09	41.03	33.80	25.17	0.62	28.08	93.13

[a] Sub G1 equals the percentage of the particles with propidium content lower than cells in G0/G1 phase; apoptosis.
[b] IC_{50} value for 72 h treatment.
[c] Fivefold IC_{50} value for 72 h treatment.

the recognition step, may be employed. Albeit conclusive effect of pentamethinium salts on cell toxicity in the presence or absence of GAGs was not found, it still did not disprove our arguments for their ability to recognize overexpressed sulfated polysaccharides on cancer cells and further allow their use for development of anticancer agents.

In addition, the biological activity of the tested compounds was assessed according their effects on the cell cycle, apoptosis, and DNA/RNA synthesis in human CCRF-CEM cells (acute lymphoblastic leukemia) after 24 h of treatment (see Table 4). The concentrations of the compounds **1**–**3** were equivalent to the IC_{50} values and their quintuples. According to this analysis, compounds **2** and **3** induced apoptosis (increase in the Sub G1 fraction) at higher concentrations (quintuple of IC_{50}). Nevertheless, we did not observe any significant changes in the distribution of cell cycle stages in the treated cells when compared to untreated control. The only recorded difference was decreased DNA synthesis in CCRF-CEM cells treated with a quintuple of IC_{50} of salts **1**–**3** and, surprisingly, enhanced RNA synthesis. However, the significance of these differences is still elusive.

3. Conclusions

In summary, we designed and synthesized a group of pentamethinium salts, **1**–**4**, with one or two positive charges and assayed them for recognition of sulfated polysaccharides. Based on the obtained results, we conclude that the synthetic ligands, mainly salt **2** with side benzothiazolium units, can be effectively used for recognition of sulfated polysaccharides. We found out that the higher number of sulfate groups together with increased density of anionic charge of sulfated polysaccharides correlated with stronger affinity to positively doubly charged salt **2**. Moreover, salt **2**, when interacting with negatively charged polysaccharides, displayed a strong correlation of the spectral response (blue shift) with the increasing degree of sulfation of the polysaccharide.

In vitro study indicated high anticancer efficiency and selectivity namely of thiodicarbocyanine **2** with two cationic charges, as well as moderate efficacy of dicarbocyanine **3** with one cationic charge. Carbocyanine **4** displayed low cytotoxicity in both control (non-malignant) and cancer cell lines. We confirmed that the type of side unit of the pentamethinium system can significantly affect the consequent biological activity.

In addition, we showed that pentamethinium salt **2** exhibits remarkably high cytotoxicity and selectivity for taxol-resistant cancer cell lines. This fact makes salt **2** the most promising potential candidate for development of a new anti-cancer agent.

4. Experimental section

4.1. Chemistry

4.1.1. Synthesis of compound *1*

The flask was charged with 2-(4-pyridyl)malondialdehyde (150 mg, 1.0 mmol), 2-methyl-3-propyl benzothiazolium iodide (640 mg, 20.1 mmol) and dry *n*-butanol (25 mL). The mixture was stirred at 110 °C for 18 h. After cooling to laboratory temperature, the mixture was filtered. The solid was washed with ethanol (3 · 5 mL) and dried in vacuum. Product **1** was obtained as green powder, 498 mg, 79%. **^{1}H NMR** (300 MHz, DMSO d_6, 25 °C): 8.94 (2H, d, J = 6.4 Hz), 8.14–7.80 (8H, m), 7.60 (2H, t, J = 8.2 Hz), 7.46 (2H, t, J = 7.6 Hz), 6.20 (2H, d, J = 13.8 Hz), 4.28 (4H, bs), 1.71 (4H, sextet, J = 7.0 Hz), 0.85 (6H, t, J = 7.0 Hz). **^{13}C NMR** (126 MHz, DMSO d_6, 25 °C): 165.9, 148.2, 143.6, 141.3, 128.2, 127.1, 125.5, 123.2, 114.0, 98.3, 47.5, 20.9, 10.8. **HRMS** for $C_{30}H_{30}N_3S_2$, calculated: 496.1876 (M^+), found: 496.1879 (M^+).

Elemental Analysis for $C_{30}H_{30}IN_3S_2$ calculated: C, 57.78; H, 4.85; N, 6.74; found: C, 57.59; H, 4.93; N, 6.67.

4.1.2. Synthesis of compound *2*

The flask was charged with cyanine dye (55 mg, 88 μmol), DMF (5 mL) and excess of methyl iodide (0.5 mL, 2 M solution in *t*-BuOMe). The mixture was heated in high-pressure ampule to 60 °C for 20 h. After cooling, the excess of methyl iodide was removed with stream of nitrogen and the rest of the solvent was evaporated. The solid was macerated with diethyl ether and filtered. Obtained solid was crystalized from hot ethanol. Product **2** was formed as metallic brown powder, 63 mg, 94%. **^{1}H NMR** (300 MHz, DMSO d_6, 25 °C): 8.96 (2H, d, J = 6.7 Hz), 7.98–8.16 (6H, m), 7.85 (2H, d, J = 6.8 Hz), 7.62 (2H, t, J = 8.2 Hz), 7.48 (2H, t, J = 8.2 Hz), 6.32 (2H, d, J = 13.8 Hz), 4.35 (7H, bs), 1.72 (4H, sextet, J = 7.0 Hz), 0.85 (6H, t, J = 7.3 Hz). **^{13}C NMR** (126 MHz, DMSO d_6, 25 °C): 166.4, 153.4, 147.9, 145.3, 141.4, 128.3, 127.8, 125.8, 125.7, 123.3, 114.2, 98.6, 47.6, 47.0, 21.1, 10.9. **HRMS** for $C_{31}H_{33}N_3S_2$ calculated: 255.6053 (M^{2+}), found: 255.6051 (M^{2+}). **Elemental Analysis** for $C_{31}H_{33}I_2N_3S_2$ calculated: C, 48.64; H, 4.34; N, 5.49; found: C, 48.83; H, 4.47; N, 5.31. **X-ray crystals** Compound **2** (50 mg) was dissolved in ethanol (5 mL) under reflux. The mixture was filtered and the filtrate was let to crystalize at laboratory temperature in a closed vial.

4.1.3. Synthesis of compound *3*

A flask was charged with quaternary salt (1600 mg, 4.86 mmol), malondialdehyde (353 mg, 2.37 mmol), dry butanol (30 mL) and three drops of triethylamine. The mixture was heated to 110 °C for 18 h. After this period, the mixture was cooled to room temperature and evaporated to dryness. The product was separated by column chromatography (eluent: chloroform/methanol 10:1, silica gel 5 · 30 cm). The product was separated as a deep blue band. Separated fraction was evaporated to dryness and to the rest, ethyl acetate was added and whole mixture was sonicated for 2 min. The pure product was separated by filtration. The yield was 347 mg, 80% in a form of deep green powder. **^{1}H NMR** (300 MHz, DMSO d_6, 25 °C): 8.78 (2H, d, J = 5.6 Hz), 8.50 (2H, d, J = 14.3 Hz), 7.67 (2H, d, J = 7.4 Hz), 7.46–7.24 (8H, m), 5.59 (2H, d, J = 14.4 Hz), 3.77 (4H, t, J = 6.7 Hz), 1.75 (12H, s), 1.55 (4H, sextet, J = 7.4 Hz), 0.74 (6H, t, J = 7.3 Hz); **^{13}C NMR** (126 MHz, DMSO d_6, 25 °C): 173.3, 151.7, 150.4, 144.0, 142.0, 141.2, 131.1, 128.5, 125.3, 125.2, 122.6, 111.5, 100.7, 49.2, 45.0, 27.0, 20.2, 11.0; **HRMS** $[M]^+$ (m/z) for $C_{36}H_{42}N_3$ calculated: 516.3373, found: 516.3377. **Elemental Analysis** for $C_{36}H_{42}IN_3$ calculated: C, 67.18; H, 6.58; N, 6.53; found: C, 67.32; H, 6.51; N, 6.74.

4.1.4. Synthesis of compound *4*

A flask was charged with pentamethinium salt **1** (100 mg, 0.015 mmol), dry DMF (7 mL) and excess of methyl iodide (1 mL). The mixture was heated to 40 °C for 18 h. After this period, the mixture was cooled to room temperature and diluted with diethyl ether (50 mL). The precipitate was filtered off and washed three times with diethyl ether (5 mL). The product was dried in vacuum. The yield was 130 mg, 100% in a form of shiny metallic green powder. **^{1}H NMR** (300 MHz, DMSO d_6, 25 °C): 9.11(2H, d, J = 6.3 Hz), 8.48 (2H, d, J = 14.6 Hz), 8.12 (2H, d, J = 6.4 Hz), 7.70 (2H, d, J = 7.4 Hz), 7.48 (2H, d, J = 8.0 Hz), 7.43 (2H, t, J = 7.9 Hz), 7.32 (2H, t, J = 7.5 Hz), 5.74 (2H, d, J = 14.0 Hz), 4.43 (3H, s), 3.98 (4H, t, J = 6.7 Hz), 1.77 (12H, s), 1.63 (4H, sextet, J = 7.1 Hz), 0.83 (6H, t, J = 7.4 Hz); **^{13}C NMR** (126 MHz, DMSO d_6, 25 °C): 174.4, 152.9, 146.0, 141.8, 141.4, 129.3, 128.5, 125.5, 122.6, 111.8, 100.1, 49.4, 47.6, 44.9, 26.9, 20.6, 11.0; **HRMS** $[M]^+$ (m/z) for $C_{37}H_{45}N_3$ calculated: 265.6801, found: 265.6804. **Elemental Analysis** for $C_{37}H_{45}I_2N_3$ C, 56.57; H, 5.77; N, 5.35 found: C, 56.32; H, 5.85; N, 5.41.

4.2. Binding study of salts **2–4**

The association constants of salts **2**–**4** with polysaccharides and sterol were measured by means of UV–Vis spectroscopy in a phosphate buffer (1 mM, H_2O:MeOH; 99:1, v/v) at pH 7.34. Conditional constants (Ks) were calculated from absorbance changes of the salts using their absorbance maximum (ΔA) by nonlinear regression in program Letagrop Spefo 2005. The used computational model was described in detail and discussed by Sillén [57]. Concentration of the used salts was 1.8 μmol L^{-1}. Concentrations of the analytes varied in the range from 0 to 0.4 mmol L^{-1}. Ks of the complexes of salts **2**–**4** with polysaccharides were calculated using the concentration of polysaccharide defined by the concentration of each basic disaccharide unit.

4.2.1. Cytotoxicity and selectivity

All cells were purchased from the American Tissue Culture Collection, unless otherwise indicated. The daunorubicin-resistant subline of CEM cells (CEM-DNR bulk) and paclitaxel-resistant subline K562-tax were selected in our laboratory by the cultivation of maternal cell lines with increasing concentrations of daunorubicin or paclitaxel, respectively [58]. The cells were maintained in exponential phase of growth in Nunc and Corning 80 cm^2 plastic tissue culture flasks and cultured in cell culture medium (DMEM and RPMI 1640 with 5g L^{-1} glucose, 2 mM l-glutamine, 100 U·mL^{-1} penicillin, 100 μg mL^{-1} streptomycin, 10% fetal calf serum, and $NaHCO_3$).

Cell suspensions were prepared and diluted according to particular cell type and expected target cell density (2500–30,000 cells·$well^{-1}$, based on the cell growth characteristics). The cells were transferred by pipette (80 μL) into 96-well microtiter plates. The inocula were pre-incubated for 24 h (at 37 °C and 5% CO_2) to stabilize. Fourfold dilutions (in 20 μL aliquots) of the tested compounds in the intended test concentrations were added to the microtiter-plate wells at time zero. All the concentrations of the tested compounds were examined in triplicates. Incubation of the cells with the tested compounds lasted for 72 h at 37 °C, in 5% CO_2 at 95% humidity. At the end of the incubation period, the cells were assayed using MTT. Aliquots of the MTT stock solution were pipetted into each well and incubated for another 4 h. After this incubation period, the produced formazan, which has arisen by mitochondrial reduction of MTT, was dissolved by addition of 10% aqueous solution of sodium dodecyl sulfate (100 μL·$well^{-1}$, pH 5.5) followed by further incubation at 37 °C overnight. The optical density (OD) was then measured at 540 nm with Labsystem iEMS Reader MF. The tumor cell inhibitory concentration (IC) of each tested compound was calculated using the following equation: IC = ($OD_{drug\ well}$/mean $OD_{control\ wells}$) × 100%. The IC_{50} value (the drug concentration lethal for 50% of the cells) was calculated from appropriate dose–response curves [58,59].

The degree of cytotoxic selectivity of the synthetic compounds for cancer cell lines is expressed as selectivity index (SI). SI is equal to IC_{50} of a pure compound in a normal cell line, what is divided by IC_{50} of the same pure compound in a cancer cell line. The IC_{50} is the concentration required to kill 50% of the cell population, what is in agreement with our previously published work [49,50].

4.2.2. Transfection assays

Transfection assays in human colorectal carcinoma cells. HCT 116 cells were seeded in 24-well plates in DMEM supplemented with 10% FBS one day before transfection to reach semi-confluent state. Cells were transfected with 0.6 mg reporter plasmid NF-κB Luc, and 0.1 mg control plasmid (pRL-TK) using polyethylenimine (PEI) method [60]. 24 h after transfection cells were washed and further cultivated in fresh media with addition either vehicle (0.1% DMSO), H_2O_2 (positive control) or salts **2** and **4** for indicated times and concentrations. Cell lysates were assayed for firefly luciferase activities and normalized against the activities of cotransfected *Renilla* luciferase. Ratios of the two luciferase activities were expressed as fold activation relative to vehicle control. Reported data are representative results obtained from four independent experiments.

4.2.3. Western blot analysis

HCT116 cells seeded at density $3 \cdot 10^{-5}$ per 35 mm dish were the following day exposed to treatment of 10 μM salt **2** for indicated times, vehicle (0.1% DMSO) and 500 μM H_2O_2 (positive control for NF-κB activation). After the elapsed periods, the cells were lysed by adding 150 μL of 1x sample buffer [50 mM Tris (pH 6.8), 1% SDS, 10% glycerol, 72 mM mercaptoethanol, 0.01% bromophenol blue), disintegrated by ultrasound of 1–2 W for 5 s and boiled for 5 min. Cell lysates were resolved by 10% SDS-polyacrylamide gel electrophoresis (SDS-PAGE) followed by electrophoretic transfer to Hybond ECL nitrocellulose membrane (Amersham). To block non-specific antibody binding and reduce background signal, blots were incubated for 1 h in 5% nonfat dry milk-Tris buffered saline with 0.1% Tween-20 (TBST) and then with specific antibody in 5% BSA (bovine serum albumin) at 4 °C overnight. Subsequently, the blot was washed 3 times with washing buffer and incubated with secondary antibody (goat anti-rabbit conjugated with horseradish peroxidase, Amersham) for 1 h. The membrane was washed another 5 times, developed in ECL reagents (Amersham), and exposed to X-ray film (Agfa). Activity of Phospho-NF-κB p65 (Ser536) antibody (Cell Signaling Technology #3033) was assayed at first and then the membrane was stripped and reprobed with antibody to total NF-κB p65 (Cell Signaling Technology #4764). Equal protein loading was verified by Ponceau S staining and β-actin reprobing.

4.2.4. Dependence of pentamethinium salts localization kinetics on GAGs presence

Cell mutant deficient in xylosyltransferase, pgsA-745, and its parental cell line, CHO-K1, were seeded in glass bottom dishes for live-cell microscopy (Ibidi, Germany) and left to adhere overnight. The cells were rinsed twice with PBS and exposed to pentamethinium salts in complete medium. The cells were incubated with 50–500 nM **1**–**4** for 10 min. up to 24 h, washed with phosphate buffer saline (PBS) and the medium was replaced with medium without phenol red. Then, fluorescence emission of the compounds was monitored by microscopy.

Similar set-up was used for A549 cells, with the difference that cells representing GAGs deprived cells, were cultivated and assayed in medium containing 50 mM sodium chlorate, which should remove surface GAGs from the cells according to Schowalter et al. [56].

4.2.5. Dependence of pentamethinium salts cytotoxicity on GAGs presence

Cell suspensions of pgsA-745, CHO-K1, sodium chlorate treated, and non-treated A549 were seeded in 96-well plates (5000 cells·$well^{-1}$) and pre-incubated for 24 h (at 37 °C and 5% CO_2) to stabilize. The tested compounds in the intended test concentrations (0–50 μM) were added to the microtiter-plate wells in complete growth media at time zero in quadruplicates and grown in standard physiological conditions. After 24, 48 and 72 h, the media was replaced with fresh media without phenol red with WST-1 (according to the manufactures protocol) and incubated for another 2 h. Then, the absorption was measured at 450 nm. The IC_{50} value (the compound concentration lethal for 50% of the cells) was calculated from appropriate dose–response curves.

4.2.6. Live-cell fluorescence microscopy

Fluorescence microscopy of pentamethinium salts was performed in living cells by real-time fluorescence microscopy (37 °C, 5% CO_2) using inverse fluorescent microscope Olympus IX-81, Cell^R System with 60x oil immersion objective (NA 1.4; Olympus, Japan), high-stability 150 W xenon arc burner, EM-CCD camera C9100-02 (Hamamatsu, Japan) and U-DM-CY5 filter cube (Olympus, Japan).

Fluorescence microscopy video recordings of localization kinetics of pentamethinium salts in living cells were recorded in the same module as described for capturing images. Video recording was started immediately at the moment of adding the tested compound (50–500 nM concentration) using 75% light intensity, exposure time 10 ms, interval between individual frames 15 s and the total count of the recorded frames 50 (12.5 min video). The videos in Supplementary information were exported in AVI file with rate 5 frames per second.

4.2.7. Cell cycle analysis

The cell cycle analysis was performed similarly as in Brulíková et al. [61] CCRF-CEM cells were treated with the tested compounds at concentrations corresponding to IC_{50} and five times IC_{50} values ($0.07 \cdot 0.36^{-1}$ μM, $0.49 \cdot 2.43^{-1}$ μM and $0.06 \cdot 0.29^{-1}$ μM for **1**–**3**, respectively) for 24 h. After the incubation period, the cells were pelleted, washed in phosphate buffered saline (PBS) and fixed with 70% ice-cold ethanol overnight at −20 °C. The cells were washed with hypotonic citrate buffer, low molecular weight apoptotic DNA was extracted and RNA was digested by RNAse (50 μg mL^{-1}). The cells (DNA labeled with propidium iodide; 0.1 mg mL^{-1}) were analyzed by flow cytometer at 488 nm (Becton Dickinson). Half of each sample was used for antibody labeling of phosphorylated histone $H3^{Ser10}$ (flow cytometry analysis of mitotic cells). The cell cycle data were analyzed in ModFitLT (Verity) software.

4.2.8. Analysis of RNA synthesis by flow cytometry

The RNA synthesis in cells was analyzed by flow cytometry similarly as described in Brulíková et al. [61]. This method is based on immunocytochemical detection of *in vitro* incorporated of 5′-bromouridine (BrU). CCRF-CEM cells were treated by salts **1**–**3** likewise for the cell cycle analysis. 5-bromo-20-deoxyuridine (BrdU; 10 μM) was added to cell media for 30 min, then the cells were harvested, washed with PBS and fixed with 1% paraformaldehyde, 0.05% NP-40 in PBS for 15 min. The cells were store at 4 °C overnight, washed with ice-cold 1% glycine in PBS (autofluorescence quenching) and again with PBS. The labelling was performed by primary monoclonal anti-BrdU antibody (1 mg mL^{-1}; Exbio, Czech Republic) for 30 min at room temperature. The cells were washed with PBS incubated with secondary anti-mouse IgG-FITC antibody (4 mg mL^{-1}, Sigma, Czech Republic) for 30 min. Then cells were fixed with 1% paraformaldehyde, 0.05% NP-40 in PBS for 15 min, washed with ice-cold 1% glycine in PBS, then with pure PBS, incubated with propidium iodide (0.1 mg mL^{-1}) and RNAse A (0.5 mg mL^{-1}) for 1 h in dark. Flow cytometry analysis was performed using a 488 nm single beam laser (Becton Dickinson).

Acknowledgements

This work was supported by National Sustainability Program II [Project BIOCEV-FAR; LQ1604]; Project "BIOCEV" [CZ.1.05/1.1.00/02.0109]; Charles University in Prague [UNCE 204064, Progress Q26/LF1 and Q27/LF1]; and Specific University Research [MSMT-SVV-260367, MSMT No 20-SVV/2017 and JIGA 2017 UCT grant 2017]. Further, this work was supported by the Ministry of Education, Youth and Sports of CR LO 1304, partially also by "EATRIS-CZ" (LM2015064) and by the Grant Agency of the Czech Republic GA17-07822S.

Appendix A. Supplementary material

Supplementary data associated with this article can be found, in the online version, at https://doi.org/10.1016/j.bioorg.2018.02.011.

References

[1] (a) J.E. Trosko, R.J. Ruch, Cell-cell communication in carcinogenesis, Front. Biosci. 15 (1998) d208–236. (b) K.S. Khabar, Post-transcriptional control of cytokine gene expression in health and disease, J. Interferon. Cytokine Res. 34 (2014) 215–219.
[2] C.J. Van der Schyf, The use of multi-target drugs in the treatment of neurodegenerative diseases, Expert Rev. Clin. Pharmacol. 4 (2011) 293–298.
[3] R. Morphy, Z. Rankovic, Fragments, network biology and designing multiple ligands, Drug Discov. Today 12 (2007) 156–160.
[4] R. Moreno-Sánchez, E. Saavedra, S. Rodríguez-Enríquez, J.C. Gallardo-Pérez, H. Quezada, H.V. Westerhoff, Metabolic control analysis indicates a change of strategy in the treatment of cancer, Mitochondrion 10 (2010) 626–639.
[5] C.M. Lee, T. Tanaka, T. Murai, M. Kondo, J. Kimura, W. Su, T. Kitagawa, T. Ito, H. Matsuda, M. Miyasaka, Novel chondroitin sulfate-binding cationic liposomes loaded with cisplatin efficiency suppress the local growth and liver metastasis of tumor cells *in vivo*, Cancer Res. 62 (2002) 4282–4288.
[6] J. Králová, J. Koivukorpi, Z. Kejík, P. Poučková, E. Sievänen, E. Kolehmainen, V. Král, Porphyrin–bile acid conjugates: from saccharide recognition in the solution to the selective cancer cell fluorescence detection, Org. Biomol. Chem. 6 (2008) 1548–1552.
[7] Z. Kejík, T. Bříza, J. Králová, P. Martásek, V. Král, Selective recognition of saccharide type tumor marker with natural and synthetic ligands: new trend in cancer diagnosis, Anal. Bioanal. Chem. 398 (2010) 1865–1870.
[8] G.W. Yip, M. Smollich, M. Götte, Therapeutic value of glycosaminoglycans in cancer, Mol. Cancer Ther. 5 (2006) 2139–2148.
[9] C.C. Lopes, C.P. Dietrich, H.B. Nader, Specific structural features of syndecans and heparan sulfate chains are needed for cell signaling, Braz. J. Med. Biol. Res. 39 (2006) 157–167.
[10] R. Sasisekharan, Z. Shriver, G. Venkataraman, U. Narayanasami, Roles of heparan-sulphate glycosaminoglycans in cancer, Nat. Rev. Cancer 2 (2002) 521–528.
[11] C. Malavaki, S. Mizumoto, N. Karamanos, K. Sugahara, Recent advances in the structural study of functional chondroitin sulfate and dermatan sulfate in health and disease, Connect. Tissue Res. 49 (2008) 133–139.
[12] X. Jiang, J.R. Couchman, Perlecan and tumor angiogenesis, J. Histochem. Cytochem. 51 (2003) 1393–1410.
[13] Z. Zhou, J. Wang, R. Cao, H. Morita, R. Soininen, K.M. Chan, B. Liu, Y. Cao, K. Tryggvason, Impaired angiogenesis, delayed wound healing and retarded tumor growth in perlecan heparan sulfate-deficient mice, Cancer Res. 64 (2004) 4699–4702.
[14] P. Westermark, Aspects on human amyloid forms and their fibril polypeptides, FEBS J. 272 (2005) 5942–5949.
[15] Y.H. Teng, R.S. Aquino, P.W. Park, Molecular functions of syndecan-1 in disease, Matrix Biol. 31 (2012) 3–16.
[16] A.M. Vogt, F. Pettersson, K. Moll, C. Jonsson, J. Normark, U. Ribacke, T.G. Egwang, H.P. Ekre, D. Spillmann, Q. Chen, M. Wahlgren, Release of sequestered malaria parasites upon injection of a glycosaminoglycan, PLoS Pathog. 2 (2006) e100.
[17] T.R. Rudd, A. Hughes, J. Holman, V. Solari, O. Ferreira Ede, R.M. Domingues, E.A. Yates, Heparan sulphate, its derivatives and analogues share structural characteristics that can be exploited, particularly in inhibiting microbial attachment, Braz. J. Med. Biol. Res. 45 (2012) 386–391.
[18] W. Zhu, S. Fu, Y. He, J. Li, G. Liang, Amino acid substitutions in the E2 glycoprotein of Sindbis-like virus XJ-160 confer the ability to undergo heparan sulfate-dependent infection of mouse embryonic fibroblasts, Virol. J. 7 (2010) 225–231.
[19] U. Lindahl, L. Kjellén, Pathophysiology of heparan sulphate: many diseases, few drugs, J. Inter. Med. 273 (2013) 555–571.
[20] J. Liu, S.C. Thorp, Cell surface heparan sulfate and its roles in assisting viral infections, Med. Res. Rev. 22 (2002) 1–25.
[21] J. van Horssen, P. Wesseling, L.P. van den Heuvel, R.M. de Waal, M.M. Verbeek, Heparan sulphated proteoglycans in Alzheimer's disease and amyloid-related disorders, Lancet Neurol. 2 (2003) 482–492.
[22] T. Lashley, J.L. Holton, M.M. Verbeek, A. Rostagno, M. Bojsen-Møller, G. David, J. van Horssen, H. Braendgaard, G. Plant, B. Frangione, J. Ghiso, T. Revesz, Molecular chaperons, amyloid and preamyloid lesions in the BRI2 gene-related dementias: a morphological study, Neuropathol. Appl. Neurobiol. 32 (2006) 492–504.
[23] S. Bussini, L. Meda, E. Scarpini, E. Clementi, G. Conti, M. Tiriticco, N. Bresolin, P. Baron, Heparan sulfate proteoglycan induces the production of NO and TNF-α by murine microglia, Immun. Ageing 2 (2005) 11–20.
[24] F. Noborn, P. O'Callaghan, E. Hermansson, X. Zhang, J.B. Ancsin, A.M. Damas, I. Dacklin, J. Presto, J. Johansson, M.J. Saraiva, E. Lundgren, R. Kisilevsky, P. Westermark, J.P. Li, Heparan sulfate/heparin promotes transthyretin fibrillization through selective binding to a basic motif in the protein, Proc. Natl. Acad. Sci. USA 108 (2011) 5584–5589.

[25] E. Elimova, R. Kisilevsky, J.B. Ancsin, Heparan sulfate promotes the aggregation of HDL-associated serum amyloid A: evidence for aproamyloidogenic histidine molecular switch, FASEB J. 23 (2009) 3436–3448.
[26] J.Y. Suk, F. Zhang, W.E. Balch, R.J. Linhardt, J.W. Kelly, Heparin accelerates gelsolin amyloidogenesis, Biochemistry 45 (2006) 2234–2242.
[27] H. Shimizu, M. Ghazizadeh, S. Sato, T. Oguro, O. Kawanami, Interaction between beta-amyloid protein and heparan sulfate proteoglycans from the cerebral capillary basement membrane in Alzheimer's disease, J. Clin. Neurosci. 16 (2009) 277–282.
[28] R. Copeland, A. Balasubramaniam, V. Tiwari, F. Zhang, A. Bridges, R.J. Linhardt, D. Shukla, J. Liu, Using a 3-O-sulfated heparin octasaccharide to inhibit the entry of herpes simplex virus type 1, Biochemistry 47 (2008) 5774–5783.
[29] J. Liu, L.C. Pedersen, Anticoagulant heparan sulfate: structural specificity and biosynthesis, Appl. Microbiol. Biotechnol. 74 (2007) 263–272.
[30] X. Xu, Y. Dai, Heparin: an intervenor in cell communication, J. Cell Mol. Med. 14 (2010) 175–180.
[31] L.M. Salonen, M. Ellermann, F. Diederich, Aromatic rings in chemical and biological recognition: energetics and structures, Angew. Chem. Int. Ed. Engl. 50 (2011) 4048–4842.
[32] A.T. Wright, Z. Zhong, E.V. Anslyn, A functional assay for heparin in serum using a designed synthetic receptor, Angew. Chem. Int. Ed. Engl. 44 (2005) 5679–5682.
[33] Z. Zhong, E.V. Anslyn, A colorimetric sensing ensemble for heparin, J. Am. Chem. Soc. 124 (2002) 9014–9015.
[34] W. Sun, H. Bandmann, T.A. Schrader, A fluorescent polymeric heparin sensor, Chemistry 13 (2007) 7701–7707.
[35] T. Bříza, Z. Kejík, I. Císařová, J. Králová, P. Martásek, V. Král, Optical sensing of sulfate by polymethinium salt receptors: colorimetric sensor for heparin, Chem. Commun. (Camb.) 16 (2008) 1901–1903.
[36] T. Bříza, Z. Kejík, J. Králová, P. Martásek, V. Král, Synthesis of unsymmetric cyanine dye via merocyanine and their interaction with DNA, Coll. Czech. Chem. Commun. 74 (2009) 1081–1090.
[37] R.M. El-Shishtawy, P.A. Almeida, A new Vilsmeier-type reaction for one-pot synthesis of pH sensitive fluorescent cyanine dyes, Tetrahedron 62 (2006) 7793–7798.
[38] A. Nakayama, F. del Monte, R.J. Hajjar, J.V. Frangioni, Functional near-infrared fluorescence imaging for cardiac surgery and targeted gene therapy, Mol. Imag. 1 (2002) 365–377.
[39] K.P. Ravindra, J. Nadine, C. Yihui, P.D. Mahabeer, Cyanine-based compounds for tumor imaging with and without photodynamic therapy, in: R.R. Gupta, L. Strekowski (Eds.), Heterocyclic Polymethine Dyes. Synthesis, Properties and Applications, Springer-Verlag, Berlin Heidelberg, 2008, pp. 41–74.
[40] S. Rimpelová, T. Bříza, J. Králová, K. Záruba, Z. Kejík, I. Císařová, P. Martásek, T. Ruml, V. Král, Rational design of chemical ligands for selective mitochondrial targeting, Bioconjug. Chem. 24 (2013) 1445–1454.
[41] S. Bamba, A. Andoh, H. Ban, H. Imaeda, T. Aomatsu, A. Kobori, Y. Mochizuki, M. Shioya, T. Nishimura, O. Inatomi, M. Sasaki, Y. Saitoh, T. Tsujikawa, Y. Araki, Y. Fujiyama, Dig. Dis. Sci. 57 (2012) 327–334.
[42] I. Capila, N.S. Gunay, Z. Shriver, G. Venkataraman, Methods for structural analysis of heparin and heparan sulfate, in: H.G. Garg, R.J. Linhardt, C.A. Hales (Eds.), Chemistry and Biology of Heparin and Heparan Sulfate, Elsevier Ltd., 2005, pp. 55–77.
[43] A. Muthusamy, R.N. Achur, M. Valiyaveettil, S.V. Madhunapantula, I. Kakizaki, V.P. Bhavanandan, C.D. Gowda, Glycobiology 14 (2004) 635–645.
[44] N.K. Matheson, Stud. Nat. Prod. Chem. Part G 26 (2002) 1113–1173.
[45] I. Capila, R. Sasisekharan, Methods for analysis of hyaluronan and its fragments, in: G.H. Garg, C.A. Hales (Eds.), Chemistry and Biology of Hyaluronan, Elsevier Ltd., 2004, pp. 21–40.
[46] M. Liu, A. Kira, H. Nakahara, Two-dimensional aggregation of a long-chain thiacarbocyanine dye monolayer on polyanion subphases, J. Phys. Chem. 100 (1996) 20138–20142.
[47] T.D. Slavnova, A.K. Chibisov, H. Görner, Photoprocesses of thiacarbocyanine monomers, dimers, and aggregates bound to polyanions, J. Phys. Chem. A 106 (2002) 10985–10990.
[48] J. van Meerloo, G.J. Kaspers, J. Cloos, Cell sensitivity assays: the MTT assay, Methods Mol. Biol. 731 (2011) 237–245.
[49] R.B. Badisa, S.F. Darling-Reed, P. Joseph, J.S. Cooperwood, L.M. Latinwo, C.B. Goodman, Selective cytotoxic activities of two novel synthetic drugs on human breast carcinoma MCF-7 cells, Anticancer Res. 29 (2009) 2993–2996.
[50] M. Al-Qubaisi, R. Rozita, S.K. Yeap, A.R. Omar, A.M. Ali, N.B. Alitheen, Selective cytotoxicity of goniothalamin against hepatoblastoma HepG2 cells, Molecules 16 (2011) 2944–2959.
[51] N. Ferrandiz, J. Martin-Perez, R. Blanco, D. Donertas, A. Weber, M. Eilers, P. Dotto, M.D. Delgado, J. Leon, HCT116 cells deficient in p21(Waf1) are hypersensitive to tyrosine kinase inhibitors and adriamycin through a mechanism unrelated to p21 and dependent on p53, DNA Repair (Amst.) 8 (2009) 390–399.
[52] Y. Lu, L. Jamieson, A.R. Brasier, A.P. Fields, NF-kappaB/RelA transactivation is required for atypical protein kinase C iota-mediated cell survival, Oncogene 20 (2001) 4777–4792.
[53] B. Paule, S. Terry, L. Kheuang, P. Soyeux, F. Vacherot, A. de la Taille, The NF-kappaB/IL-6 pathway in metastatic androgen-independent prostate cancer: new therapeutic approaches?, World J Urol. 25 (2007) 477–489.
[54] Y. Fan, J. Dutta, N. Gupta, G. Fan, C. Gélinas, Regulation of programmed cell death by NF-kappaB and its role in tumorigenesis and therapy, Adv. Exp. Med. Biol. 615 (2008) 223–250.
[55] K.M. Ryan, M.K. Ernst, N.R. Rice, K.H. Vousden, Role of NF-kappaB in p53-mediated programmed cell death, Nature 404 (2000) 892–897.
[56] R.M. Schowalter, D.V. Pastrana, C.B. Buck, Glycosaminoglycans and sialylated glycans sequentially facilitate merkel cell polyomavirus infectious entry, PLoS Pathog. 7 (2011) e1002161.
[57] L.G. Sillén, High-speed computers as a supplement to graphical Methods. III. Twist matrix methods for minimizing the error-square sum in problems with many unknown constants, Acta. Chem. Scand. 18 (1964) 1085–1098.
[58] V. Noskova, P. Dzubak, G. Kuzmina, A. Ludkova, D. Stehlik, R. Trojanec, A. Janostakova, G. Korinkova, V. Mihal, M. Hajduch, *In vitro* chemoresistance profile and expression/function of MDR associated proteins in resistant cell lines derived from CCRF-CEM, K562, A549 and MDA MB 231 parental cells, Neoplasma 49 (2002) 418–425.
[59] M. Hajdúch, V. Mihál, J. Minarík, E. Faber, M. Safárová, E. Weigl, P. Antálek, Decreased *in vitro* chemosensitivity of tumour cells in patients suffering from malignant diseases with poor prognosis, Cytotechnology 19 (1996) 243–245.
[60] P.A. Longo, J.M. Kavran, M.S. Kim, D.J. Leahy, Transient mammalian cell transfection with polyethylenimine (PEI), Methods Enzymol. 529 (2013) 227–240.
[61] L. Brulíková, P. Džubák, M. Hajdúch, M. Lachnitová, M. Kollareddy, M. Kolář, K. Bogdanová, J. Hlaváč, Synthesis of 5-[alkoxy-(4-nitro-phenyl)-methyl]-uridines and study of their cytotoxic activity, Eur. J. Med. Chem. 45 (2010) 3588–3594.